4.3 Damping Ring

4.3.1 Introduction

The fundamental role of the damping ring is to produce a low emittance beam within the repetition time of the collider system. The key issues are the damping time and the equilibrium emittances. The basic requirements to the damping rings for the three frequency options are summarized in Tab. 4.6. The small ratio of the vertical to horizontal emittances makes it easy to design the final focus system and relaxes the beam-beam effect at the collision point. The value 1% is believed to be achivable in the damping ring with the present technology.

Table 4.6: Requirements to the damping rings for the JLC-I.

Items	S-band	C-band	X-band
particles per bunch [$\times 10^{10}$]	1.75	1.11	0.65
bunches per train	55	72	90
bunch spacing [nsec]	5.6	2.8	1.4
normalized emittance $\gamma\epsilon_x[\times 10^{-6}$radm]	3.0	3.0	3.0
normalized emittance $\gamma\epsilon_y[\times 10^{-8}$radm]	3.0	3.0	3.0
repetition rate [Hz]	50	150	150

The beam energy of the damping ring is not the primary issue; it is a parameter to be optimized in the damping ring design. Generally speaking, a lower energy is better for the emittance but a higher one is preferred for the damping time. After some optimization processes taking into account the various effects such as the bunch lengthening, particle collision within a bunch (intrabeam scattering), we have decided the energy to be 1.98 GeV. (This fractional value comes from the requirement for the polarized beam. See Sec. 4.2.2.)

The emittance of the extracted beam is given by

$$\epsilon = \epsilon_i e^{-2t/\tau} + (1 - e^{-2t/\tau})\epsilon_{eq}, \tag{4.8}$$

where ϵ_i is the emittance of the injected beam, ϵ_{eq} the equilibrium emittance including the effects of intrabeam scattering, τ the horizontal or vertical damping time, and t the time the bunch stays in the ring. We assume the injected beam emittance of $\gamma\epsilon_i = 5 \times 10^{-5}$radm, which is produced by the RF gun for the electron beam and by the pre-damping ring for the positron beam. The pre-damping ring was designed to accept the positron beam with the normalized emittance 3.0×10^{-3}radm (rms) and the energy spread 1%. Its circumference is $\sim$ 110m and the damping times $\tau_x = \tau_y \leq\sim$ 4msec [13]. Thus the vertical emittance needs to be decreased by three orders of magnitude. Damping the bunch for five vertical damping times will reduce the first term of above equation by four orders of magnitude. The requirement on the vertical equilibrium emittance is then

$$\gamma\epsilon_{y,eq} \leq 2.7 \times 10^{-8}\text{radm}. \tag{4.9}$$

The required damping times are determined from the desired repetition rate (50Hz or 150Hz), the number of damping times per bunch (5) and the number of trains stored in the ring at once (N_t);

$$\tau_x, \tau_y \leq N_t/(f_{rep} \times 5) \tag{4.10}$$

We assume that the rise and fall times of the kickers be less than 60nsec. Such kickers have been already developed. The flat-top length is in the range of $\sim$ 100 to $\sim$ 300 nsec. Thus the trains must be separated by at least 60nsec. Obviously, the circumference of the ring (L_{ring}) satisfies the following inequality.

$$L_{ring} \geq c(N_b t_b + 60\text{nsec})N_t, \tag{4.11}$$

where N_b is number of bunches per pulse and t_b the bunch spacing. Since $N_b t_b \geq 60$ nsec, the ring circumference is almost determined by $N_t N_b t_b$.

The damping time is directly proportional to ϱ_B/γ^3, where ϱ_B is the local bending radius. On the other hand, the normalized emittance is inversely proportional to ϱ_B/γ^3. In order to reduce both the damping time and the normalized emittance at the same time, we have decided to introduce long wiggler sections in a zero-dispersion region. We also selected a racetrack shape to minimize the space for the dispersion suppression and matching.

Since the equilibrium emittance can be reduced by decreasing the dispersion in the bending magnets or the strength of the bends, we selected a combined function FOBO cell for the arc. The combined function bend has a strong defocussing field and is positioned at the center of a cell in order to minimize the dispersion there.

The ratio of the impedance threshold to the equilibrium normalized emittance, $(Z/n)_t/\gamma\epsilon_{x0}$, is inversely proportional to the cell length[15]. We need a 1.12m drift space in each cell. This length allows a space for sextupole magnets, steering magnets, and position monitors.

Let us consider the scaling formulas including the effects of damping wigglers. After approximations applicable to our case, we find

$$\tau_{eff} \propto \varrho_w^2/L_w, \tag{4.12}$$

where $\tau_{eff} \equiv \tau/N_t$, ϱ_w and L_w are the bending radius and the length of the wiggler. If τ_{eff} is given(=1.0msec), the impedance threshold goes as

$$(Z/n)_t \propto \theta^2 \varrho_w/L_w \propto \theta^2/\varrho_w, \tag{4.13}$$

where θ represents the bending angle per cell. Moreover, if $(Z/n)_t$ is given (=0.3Ω), the equilibrium normalized emittance behaves as

$$\gamma\epsilon_{x0} \propto L_{cell}\varrho_w/\varrho_0^2 \propto \varrho_w/\varrho_0, \tag{4.14}$$

where ϱ_0 is the bending radius of the main magnet. Conversely, if $\gamma\epsilon_{x0}$ is fixed ($=3.0\times10^{-6}$radm) instead of $(Z/n)_t$,

$$(Z/n)_t \propto \varrho_0/\varrho_w. \tag{4.15}$$

By decreasing the main bending field, one can reduce the emittance without making the impedance requirement tighter, although the cell becomes longer. Therefore, it is desirable to maximize the wiggler fields and minimize the normal bending field. In the next section we present a design which meets all the requirements described above. We can decrease both the damping time and the normalized emittance by increasing the wiggler length. This feature is one of the characteristics of our design.[16]

4.3.2 Lattice and Optics

The damping rings are designed for the three frequency options, using the same components as those developed for the Accelerator Test Facility (ATF) at KEK.[17] We describe here the detail only of the C-band option and present a table to compare the three options. The configuration of the ring is illustrated in Fig. 4.20. The ring has a circumference of 320.8m

Table 4.7: Parameters of the damping rings

Main Linac Frequency	S-band	C-band	X-band
Synchrotron Radiation per turn [MeV]	0.367	0.99	0.71
Harmonic Number	530	764	660
Total Current [mA]	410	478	405
Circumference [m]	222.5	320.8	277.1
Number of Trains	2	4	4
Number of Bunches per Train	55	72	90
Number of Particles per Bunch [10^{10}]	1.73	1.11	0.65
Longitudinal Impedance Threshold [Ω]	0.145	0.316	0.594
Repetition Rate [Hz]	50	150	150
Momentum Compaction	0.00098	0.00126	0.00140
Natural Emittance [nradm]	0.512	0.569	0.618
Horizontal Damping Time [msec]	6.13	3.54	4.04
Vertical Damping Time [msec]	8.01	4.30	5.20
Bunch Length [mm]	4.5(4.8)	4.9(5.0)	4.9(5.0)
RF Voltage (0.714GHz) [MV]	1.1	2.1	1.9
Energy Spread [10^{-4}]	8.6(9.09)	9.1(9.29)	9.14(9.24)
Touschek Lifetime [sec]	41	70	130
Emittance with Intra-beam [10^{-10}]	6.73	6.41	6.18
Horizontal Phase Advance per Cell [degree]	120	90	92
K2 values of SF and SD	33.4,-45.9	25.9,-33.4	26.3,-33.6
Necessary Total Power [MVA]	5	9	7

and a superperiodicity of two. The optical functions β_x and β_y and the dispersion function η_x for a half of the ring are plotted in Fig. 4.21. The damping times are $\tau_x = 3.54$msec and $\tau_y = 4.30$msec. This allows each train to stay in the ring for 6.2 vertical damping times when operated at 150Hz. The intrabeam scattering contribution to the emittance is about 13% of the equilibrium emittance.

Each arc consists of 30 combined-function FOBO cells. The bending angle is 6.00°, and the normalized gradient of the quadrupole magnets is 4.17m^{-2}. With the magnet aperture r=1.6cm, which is 2mm larger than the beam pipe, the pole tip field of the quadrupoles is 4.4kG. The magnet configulation in a cell is plotted with the lattice functions in Fig. 4.22.

The design of the wiggler is crucial in our design. It has the effective field 1.88T, the period $\lambda_w = 40.0$cm, and the total length 133m with the packing factor 0.36. The configuration of the wiggler section is shown in Fig. 4.23. We use 58 wigglers. A high field quality is required since the non-linear fields can reduce the dynamic aperture and cause a beam loss at the injection.

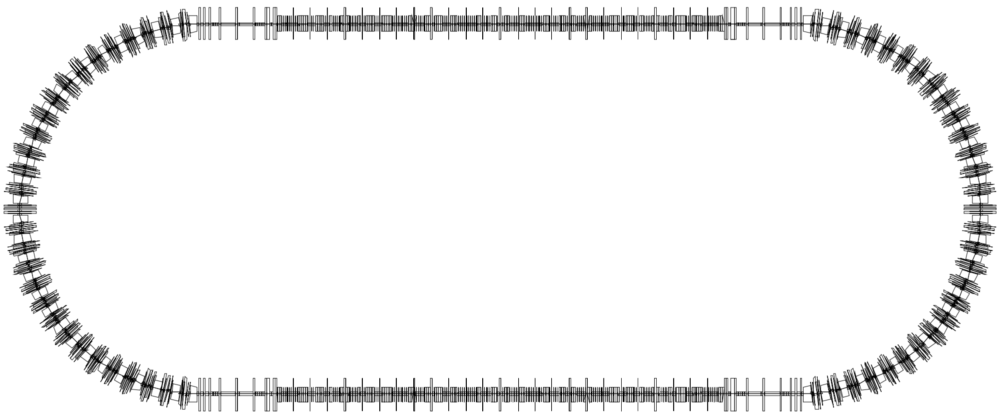

Figure 4.20: Schematic layout of the JLC damping ring.

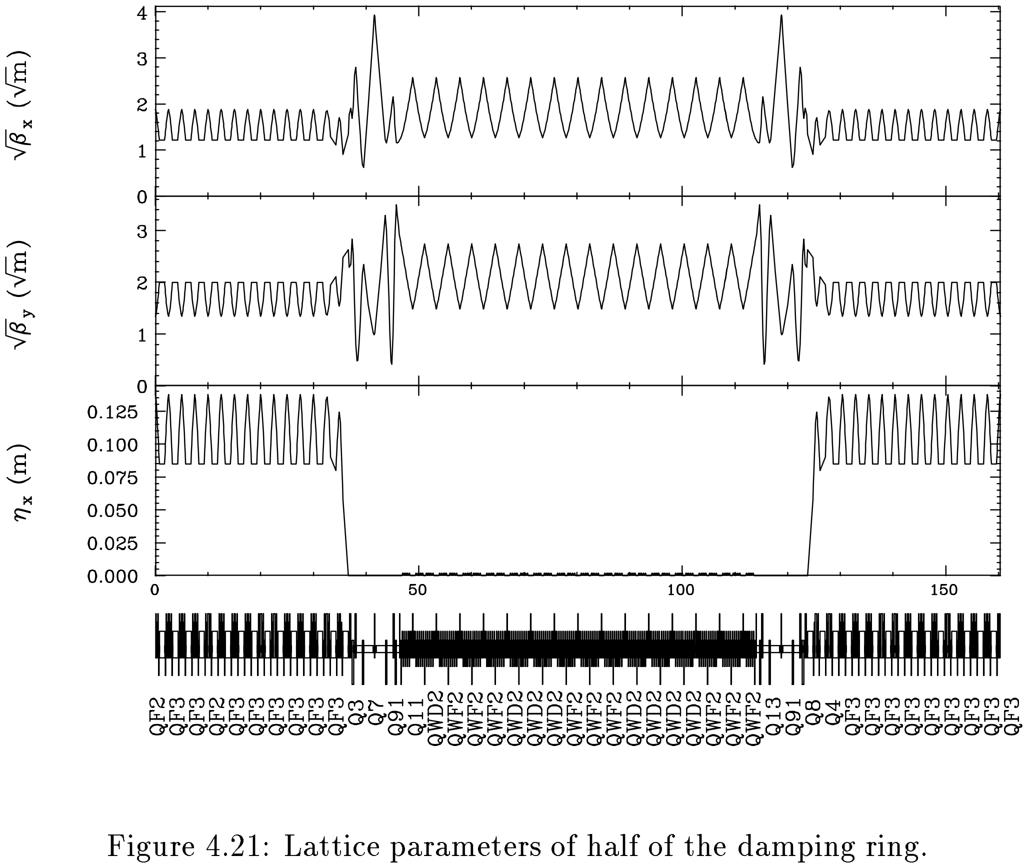

Figure 4.21: Lattice parameters of half of the damping ring.

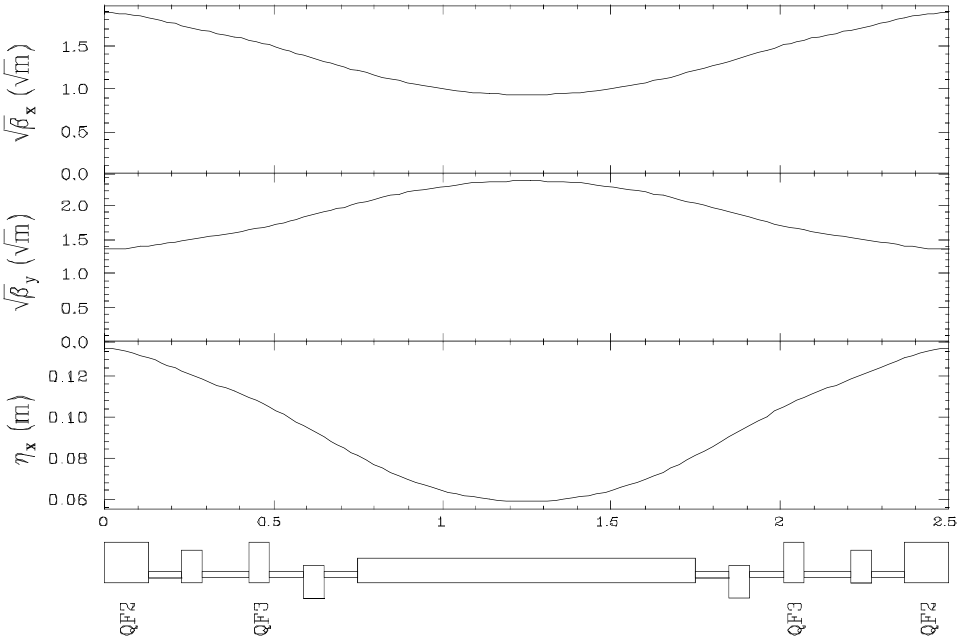

Figure 4.22: Lattice parameters of a single normal cell.

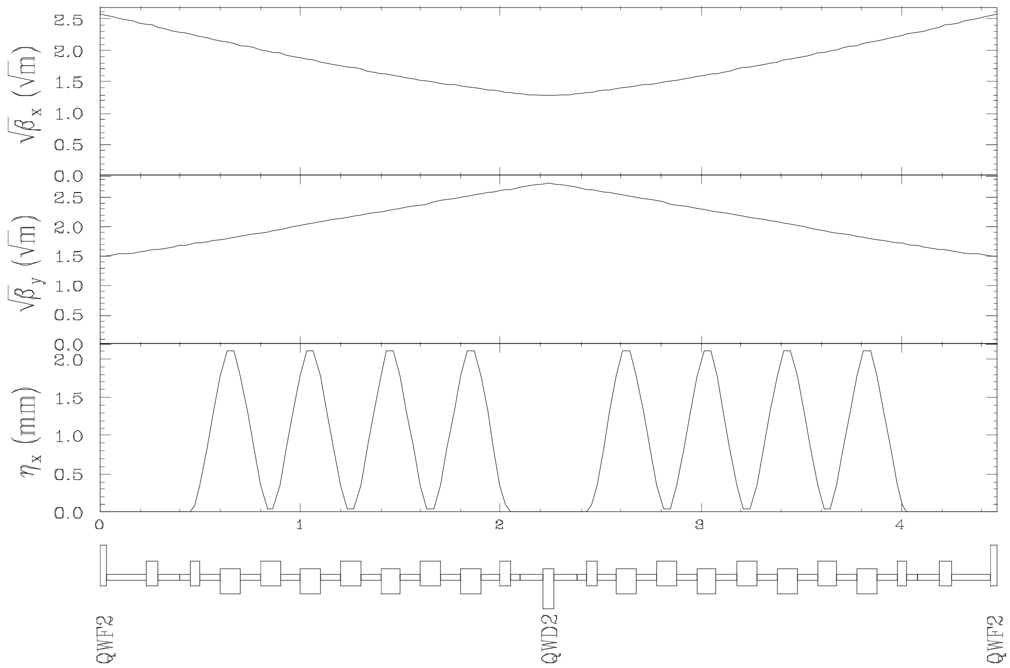

Figure 4.23: Lattice parameters of a wiggler cell.

4.3.3 Dynamic Aperture and Alignment Tolerances

Since the damped beam has a much smaller dimension than the injected beam, the requirement of the dynamic aperture comes from the size of the latter. Three times the rms size will be enough in order to avoid a significant beam loss. We will measure the dynamic aperture in terms of the horizontal equilibrium beam size σ_0. Since the injected emittance is larger than the equilibrium emittance by a factor 50/3, three sigmas of the injected beam size correspond to $13\sigma_0$ (~1.5mm). The planned beam pipe in the arcs has a 13.5mm inner radius or $\sim 22\sigma_0$.

We correct the chromaticity with only two families of sextupoles in the arcs. The integrated sextupole strengths are: $K_{2SF} = 25.9\text{m}^{-2}$ and $K_{2SD} = -33.4\text{m}^{-2}$. The results from the computer code SAD indicate that the dynamic aperture is more than $80\sigma_0$ without nonlinear fields of wigglers. It will decrease when errors and the wiggler nonlinear field are included. However, the tracking simulations made with a sinusoidal nonlinear field show that the aperture is still more than $40\sigma_0$. A result of tracking over 1000 turns using SAD is plotted in Fig. 4.24. We find that the tolerance of the magnet misalignment and the monitor setting error is 30μm vertically and 50μm horizontally and those of rotation and of the field error are 0.5mrad and 0.1%, respectively.

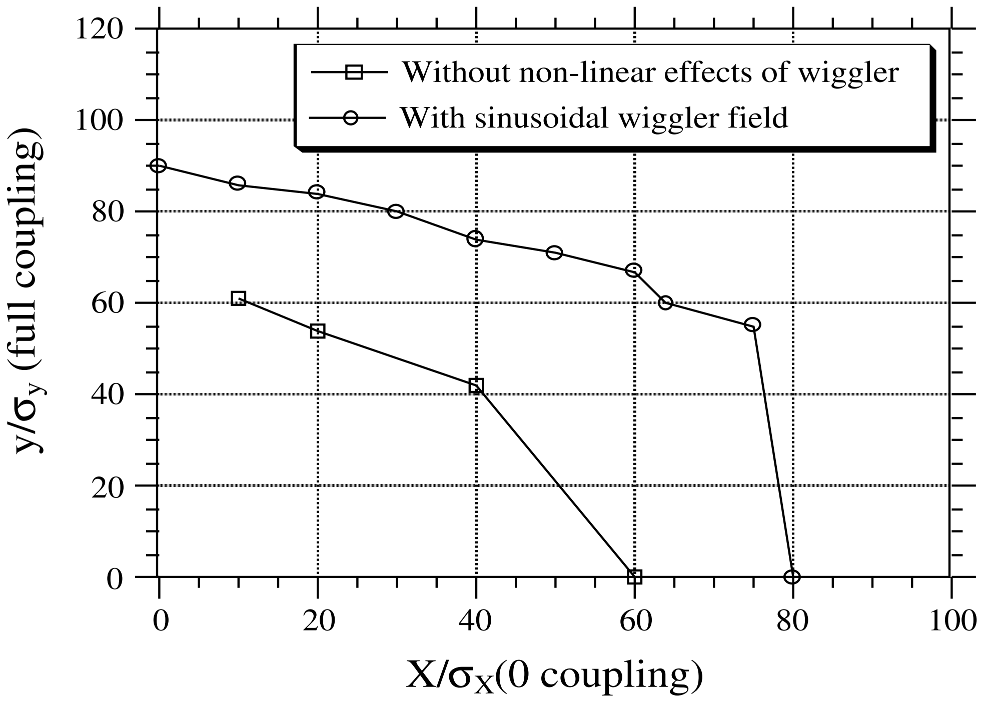

Figure 4.24: Dynamic aperture.

4.3.4 Single Bunch Instability

The short-range longitudinal wake causes the bunch lengthening. It was observed in the damping ring of the Stanford Linear Collider(SLC) [18]. This phenomenon restricts the performance of the damping ring operated at a high current. The relevant wake fields are generated at discontinuities of the vacuum chamber. Almost all the vacuum components of the JLC-I damping ring are the same as those of the ATF damping ring. For the ATF damping ring, we have estimated the wake field strength (the impedance) of the various components [19] by using the computer codes TBCI [20] and T3 [21].

Source of the Wake

The cross section of the beam duct is a circle of 27 mm in diameter and a race-track shape of 15 mm high $\times$ 47 mm wide. They are connected by tapered tubes to keep the impedance low. However, there are many other discontinuities in the ring as listed in Table. 4.8. The bellows and gate valves have an RF contact inside so that the beam does not see the discontinuous structure. The flanges have a special gasket and there is no inside gap. We use some photon absorbers to protect the bellows and other components from the irradiation of the synchrotron light. They are the largest impedance source in the ring. Therefore, it is essential to reduce the number of absorbers as far as we can. Further, another large impedance source is the RF cavity. We will use four cavities in the ring.

Table 4.8: Longitudinal Impedance evaluated by TBCI and T3.

Components	$\lvert Z_{\parallel}/n\rvert$ (Ω)	Number	$\lvert Z_{\parallel}/n\rvert^{(total)}$ (Ω)
Cavities	0.02	4	0.08
Vacuum pump holes	5.4×10^{-8}	$1.5 \times 10^5/100m$	0.01
Vacuum pump slots	6×10^{-7}	$1300/25m$	0.001
Monitor electrodes	2×10^{-5}	4×60	0.005
Bellows	3.5×10^{-4}	200	0.07
Septum chamber	6.8×10^{-4}	2	0.001
RF quadrupoles	6.4×10^{-3}	2	0.01
Transitions	1.5×10^{-3}	4	0.006
Clamp chain flanges	4×10^{-5}	100	0.004
Gate valves	8×10^{-4}	8	0.006
Photon absorbers	5×10^{-4}	200	0.10
Total			0.29

Bunch Lengthening

The typical threshold limit of the longitudinal impedance is given by [22]

$$|Z_{||}/n|_{threshold} = \frac{(2\pi)^{3/2}\sigma_\tau \alpha E \sigma_\epsilon^2}{e^2 N}, \tag{4.16}$$

where σ_τ is the r.m.s. bunch length, α the momentum compaction factor, E the beam energy, σ_ϵ the relative energy spread, and N the number of particles per bunch. The threshold impedance is 0.11Ω for the ATF damping ring and 0.17Ω for that of JLC-I, while the calculated impedance is 0.29Ω in total. The simple criterion above, however, often leads to an under-estimation of the threshold, depending on the type of impedance. Therefore, we estimated the threshold by another method, which solves the Vlasov equation and computes the growth rates of eigenmodes, taking into account the potential-well distortion and the synchrotron radiation [23, 24]. While the maximum design intensity of the JLC-I damping ring is 2×10^{10} particles per bunch, the results of the eigenmode method show that the threshold intensity is 0.9×10^{10} if we use an axially symmetric absorber along the beam axis. The threshold intensity becomes 3.5×10^{10} if we reduce the absorber impedance to 1/4. Actually, the absorber is needed only on the outer wall of the chamber and its azimuthal filling factor is 1/10, or 1/5 if it is also attached on the inner wall to keep the left-right symmetry. In addition, it seems possible to halve the number of absorbers by optimizing the cooling system of the vacuum chambers. Therefore, we think we can avoid the bunch lengthening, which will be confirmed through the ATF studies.

4.3.5 Multibunch Instabilities

Because of the high current and the large number of bunches in the ring, cures for the coupled-bunch effects have to be considered. Possible effects of the RF cavities are

1. coupled bunch instabilities caused by the accelerating mode,

2. shift of bunch position due to the beam loading,

3. coupled bunch instabilities by higher order modes.

Because of the high beam current and large circumference, the band width and the detuning frequency of the cavities should be comparable with the revolution frequency. Then the growth rate of the '-1' mode, which is excited by the tail of the impedance of the accelerating mode, may be higher than the radiation damping rate in some conditions. This instability can be avoided by a high accelerating voltage with low R/Q of the cavities. The design of our RF system will achieve this condition. Another solution is the RF feedback for the specific oscillation modes. The growth rate of the coupled-bunch motion is estimated analytically to be less than 100 s^{-1}, which is much less than the radiation damping rate. The stability of the bunches has been checked by tracking simulations of rigid bunches including the wakefield of the accelerating mode.

Since the bunches are not uniformly distributed over the ring because of the gap between the trains, each of them feels a different wakefield (beam loading) induced by the preceding bunches. The bunch energies are anyway the same so as to keep the revolution frequency unchanged. As a result, the head bunch in a train delays and tail bunch advances from the nominal positions. The shift of the positions would become comparable with the bunch length if not cured. A high accelerating voltage with low R/Q can reduce this shift, too. In addition, an RF system for beam-loading compensation will be installed to minimize the shift. This system has two cavities having different frequencies $f_{main} \pm N_t f_{rev}$, where f_{main} is the frequency of the main RF and f_{rev} the revolution frequency. The necessary peak voltage is about 50 kV. Behavior of the bunches with this beam loading compensation system has been studied by tracking simulations.

The longitudinal instabilities caused by higher-order modes (HOM) can be suppressed by the so-called 'damped cavity' (cavity with low Q values of higher order modes). The threshold Q of HOMs estimated by a tracking simulation is

$(R/Q) \times Q \times f \ \sim \ 10^4$ for each monopole mode,

where f is the frequency of each mode in GHz and R/Q is in Ω. This value agrees with analytic calculations for uniformly distributed bunches with the same total current.

The transverse instabilities can be suppressed by the damped cavity and the bunch-to-bunch tune spread within each train. The requirements are estimated by a tracking simulation as

$(R/Q)Q \sim 10^6\ (\Omega/m)$ for each transverse mode,

$\Delta\nu \sim 1 \times 10^{-3}$,

where $\Delta\nu$ is peak-to-peak betatron tune difference within a train. These values also agree with analytic results for uniformly distributed bunches with the same total current assuming that bunches in a train are decoupled because of different tunes. These requirements to the RF cavities can be satisfied as will be described later and the tune spread can be obtained by an RF quadrupole.

4.3.6 Injection and Extraction

Injection

Three septum magnets successively deflect the beam injected from the RF gun or from the pre-damping ring by $110, 132$, and 44mrad. The beam is further deflected by about 4.5mrad by a kicker magnet to match the closed orbit of the ring. The injection error will be smaller than $0.1mm$. To keep the beam loading of the cavity in the damping ring almost constant, the RF bucket which has been occupied by the just extracted bunch must be filled immediately by an injected bunch. So, the beam extraction point, the injection point, and the cavity section must be located in the ring in this order.

Extraction

The stabilization of the beam extracted from the damping ring is extremely important. The jitter has to be less than one tenth of the beam size.

The beam to be extracted is deflected by about 4.65mrad by a kicker magnet into the first septum magnet. The three septum magnets successively deflect the beam by 44, 132, and 110 mrad. For the septum magnets, DC magnets are chosen, because pulsed ones will introduce larger jitters. The pulse-to-pulse reproducibility in the total deflection angle (286mrad) is better than $\pm 3 \times 10^{-5}$.

Assuming $\beta_x \cong 10$m, the jitter tolerance on the kicker is estimated to be 5×10^{-4} [15]. In order to achieve this tolerance, we need to use a double kicker system, separated by a phase advance of π, to cancel the jitter. The first kicker will be placed in the damping ring and the second kicker in the extraction line, thus reducing the jitter into the range 10^{-4} to 5×10^{-4}. Fig. 4.25 shows a design orbit trajectory for injection and extraction.

4.3.7 Magnet System

Conceptual designs have been made for damping wigglers, combined function bends, quadrupole and sextupole magnets. The magnet specifications were determined with consideration for the available space and the cost of the magnets and power supplies. It is necessary to be able to separate upper and lower parts of quadrupoles, sextupoles, and wigglers for the installation of the vacuum chamber. For magnetic field and alignment reproducibility, these magnets should have some precise knock-pins. This reproducibility may affect the alignment accuracy of the damping ring.

The low emittance and fast damping require high-field, short-pitched wigglers. These conditions conflict each other, because a high field needs much space for coils or permanent magnets.

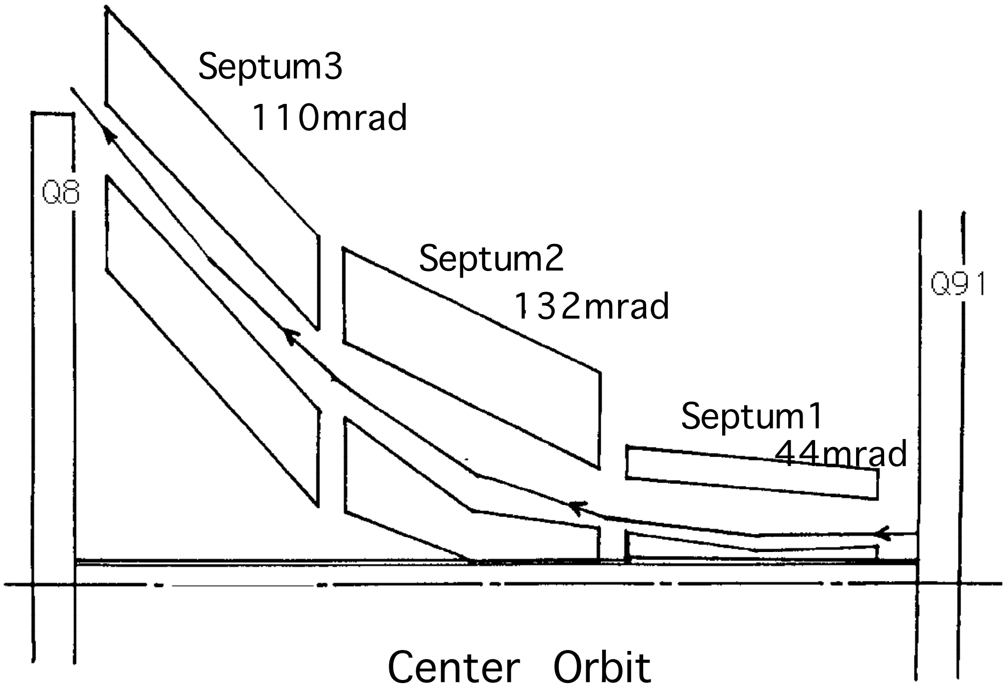

Figure 4.25: Design orbit trajectory for injection and extraction.

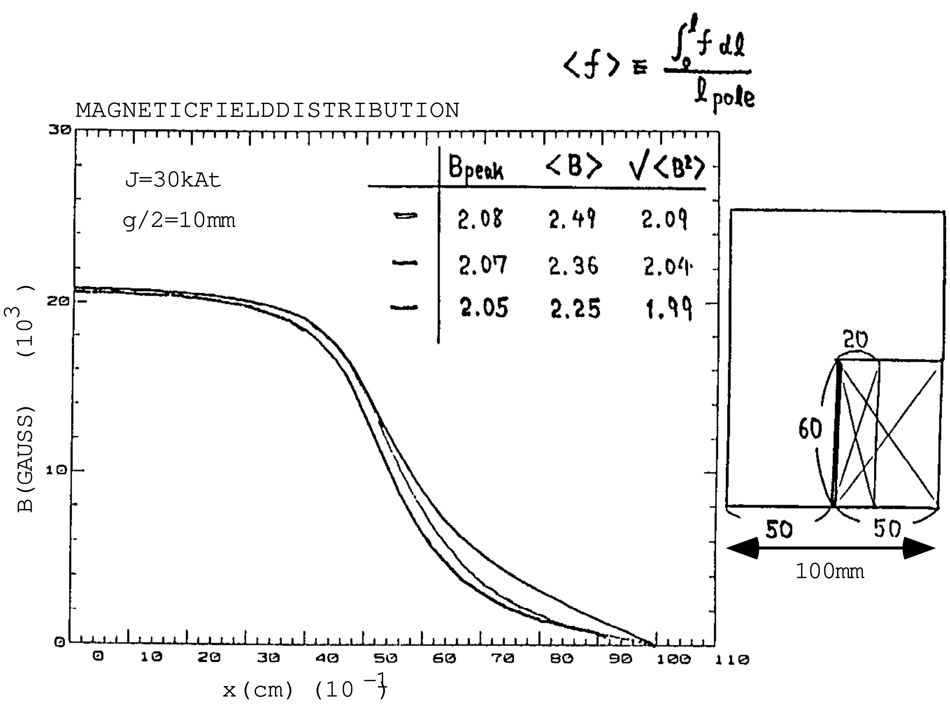

Figure 4.26: Magnetic field distribution of the wiggler.

Examining wiggler effects on the emittance, we found that the η' term is dominant and that the free space between adjacent wiggler poles has almost no effect on the emittance in the lowest order approximation. This fact eases the requirement on the wiggler pitch. Our choice of the pitch is 0.4m. Since we do not know yet much about the field degradation of assembled permanent magnets and the durability against radiations and heat, we adopt conventional electric magnets with compact coil fed with intense currents. A field as high as $B_{peak} \sim B_{eff} \sim 2$T is obtainable ($B_{eff}$ is defined by $[\int B^2 ds/l_{pole}]^{1/2}$), but we reduced it to $1.8 \sim 1.9$T with a consideration of the power consumption. Fig. 4.26 shows the magnetic field distribution of the wiggler.

Introducing combined function bends having defocusing quadrupole field, we can make the D parameter (which appears in the expression for the damping partition) negative, which reduces the transverse emittance. This combined bend must be of sector type, otherwise the beam feels a varying field as much as 15% of B_0 in a 1m bend. A logarithmic pole profile is obtained for the sector-type combined function bend by solving the Poisson equation in the cylindrical coordinate. The field distribution and its dependence on the coil position, shimming, and possible manufacturing errors were studied by using the code POISSON. The coils must be of saddle shape to save the space between the magnet poles. In determining the coil dimensions the alignment processes must also be taken into consideration.

The field will be measured by the orthodox methods, rotating coils for quadrupoles and sextupoles and flip coils for bends. The use of a laser with quadrant photo-diodes will be effective in positioning and alignment processes.

4.3.8 RF System

The RF system should provide sufficient accelerating voltage not only to compensate the radiation loss but also to obtain required energy acceptance and the small bunch length. Using twelve single-cell cavities, total voltage of about 3 MV will be obtained. The shunt impedance is estimated to be 3.9 MΩ per cavity. To obtain voltage of each cavity of more than 0.25 MV, the wall power loss will be 16 kW per cavity. With the power 50 kW per cavity to be gained by the beam, the total required power will be 800 kW or 66 kW per cavity. This power will be supllied by three klystrons. Each klystron will feed 270 kW to four cavities. The band width of the power source will be much broader than 2 MHz for quick RF control to avoid transient beam instabilities at injection and extraction of beams. The RF frequency has been chosen to be 714 MHz which is 1/4 of the frequency of the injector linac. Possibility of higher frequency of 1428 MHz has been studied, but the lower frequency is preferred regarding the coupled-bunch instabilities by the accelerating mode of the cavities and the non-uniform beam loading. With a lower frequency, the growth rate will be smaller, because a smaller detuning frequency is needed. The ratio of the voltage to R/Q is also smaller and, therefore, the position shift will be less.

The requirement of low Q-values of higher order modes will be met using damped cavities. Wakefields of higher order modes induced in each cavity will be extracted through four rectangular wave guides whose cut-off frequency is chosen to be between the accelerating mode and the lowest higher order mode. This cavity can achieve the required Q-values (20 for TM_{011} mode and about 100 for other modes).

RFQ to cure the coupled-bunch betatron oscillations

In order to avoid transverse coupled-bunch motions, a spread of the betatron tune among the bunches in a train is needed. The peak-to-peak tune difference of about 0.001 will be obtained using RF-quadrupoles. Tracking simulations have shown that this is enough to suppress the instability.

4.3.9 Instrumentation

Monitor System

The beam position monitors are chosen to be of electrostatic type with four button-like electrodes because of low coupling impedance, low cost, and simple structure. The position monitor system is designed to achieve the resolution of 10μm (rms) in order to correct the 3mm-dispersion in the wiggler section. The circuits for the signal processing are being designed as single-pass BPM. Time division processing will be used to reduce the total cost of the circuit and to increase system reliability without coaxial switches. Four signals from the button electrodes are combined through delay coaxial cables by an RF combiner. The adequate low frequency component from the combiner is transmitted to a flash ADC with four gates. In order to correct the dispersion, we measure the dispersion by comparing the closed orbit distortions under different RF frequencies (Δf_{RF} = 10kHz). Then, the change of the orbit is 6.4μm. Therefore, we need to average at least ten position data to get a resolution below 3μm. The data will be accumulated into the buffer memory of the flash ADC.

Alignment System

A prototype of the support table for the ATF damping ring was designed and ordered. It is 2.4m long and 1.0m wide and has three legs, each having a vertical and a horizontal mover with stepping resolution of 5μm. The table also has three hydrostatic levellers, with which the vertical table position can be measured. The horizontal position will be measured by using two sets of a quadrant photo-diode and a laser diode.

After field mapping, all the magnets in one normal cell are mounted on the table. This can be done with an accuracy better than 20μm, since various high techniques are available for alignment over a few meters. The mounting must be stable enough because we need to move the table to the right place after mounting. As stated in Sec. 4.3.7, the upper and lower parts of every magnet are made separable for the installation of the vacuum chambers. We need to check whether the magnets are shifted during the separation and joining. These problems will be studied in the ATF construction.

The alignment of the table itself along the design orbit is expected to be done in the accuracy of 20μm horizontally, 30μm vertically, and 0.3 mrad in rotation.

Beam Instrumentation after beam extraction

To maintain the high luminosity operation, we need to measure often the emittance of the extracted beam. Since the beam from the damping ring is very small vertically, the carbon wire monitor which is used near the SLC interaction point is a good candidate. We are investigating a high resolution wire scanner with the 4μm carbon wire. By using this high resolution wire scanner, the vertical and horizontal emittances of the extracted beam will be measured. To confirm the vertical ultra-low emittance is essential for advanced linear colliders.

4.3.10 Vacuum system

The main purpose of the damping ring is to get a low emittance beam. The vacuum system must be designed to achieve such pressure that does not disturb the beam emittance through beam-gas scattering. Scattering effect has been evaluated by several persons [25, 26, 27]. Allowing a vertical emittance growth of 10%, we need an average pressure of the ring below 6×10^{-6} (Pa). The gas desorption in an electron storage ring is dominantly induced by the irradiation of synchrotron radiation (SR). The density of the SR photons at the chamber wall will reach 2×10^{19} and 1×10^{19} photons/m/s in the wiggler and arc sections, respectively. We assume that the photo-desorption rate of the chamber is 1×10^{-5} molecules per photon. Then we must achieve the pumping speed of 140 and 70 l/s/m for two sections respectively. Basic design concepts of the vacuum system are as follows.

1. Make all vacuum chambers by the extrusion of aluminum alloy. They will be baked to 150 °C for 24 hours before assembly at the beam line, but will not be baked *in situ*.

2. Connect vacuum chambers by clamp-chain flanges and bellows. The chambers will not be weld *in situ* due to the limitation of the connection space.

3. Localize the synchrotron radiation by using photon absorbers, especially in the arc section. It has a merit that we can minimize the area of high gas desorption.

4. The general cross section of the beam duct is a circle of 27 mm in diameter, except for cavities and absorbers. The wiggler chamber has a race-track shape, 15 mm high × 47 mm wide. These chambers must be connected to form a smooth transition keeping the impedance contribution low.

5. Use two types of bellows with race-track and circular apertures that match the chamber's. Insert the RF shield into the bellows and gate valves.

6. Install a cold-cathode gauge to each cell to monitor the pressure of the ring. The additional information will be obtained by monitoring the ion-pump currents.

Most of the above components are similar to those in preparation for the ATF damping ring and, therefore, will be tested soon.

Vacuum Chambers

The cross sectional view of the wiggler chamber is shown in Fig. 4.27 (a). The beam duct has cooling channels on both horizontal sides. Along the beam duct, two side channels for non-evaporable getter (NEG) pumps are installed. They are connected with the beam duct through slots that are created in the space between the cooling channel and the outer chamber wall. Three pumping ports are provided on the inner side of the ring to install ion pumps, some vacuum gauges and the roughing pump systems. The cross section of a bending chamber is shown in Fig. 4.27 (b). The bending magnet is a combined type and the gap between the magnet poles is open to the outside of the ring. We will add an antechamber to the beam chamber to localize the area irradiated by SR photons. Ion pumps and NEG pumps will be installed near the photon absorber to evacuate the out-gas effectively. With the beam current of 450 mA (C-band design), the maximum linear power density along the beam duct becomes 1.5 kW/m for both the wiggler and arc sections. These chambers are cooled down by water.

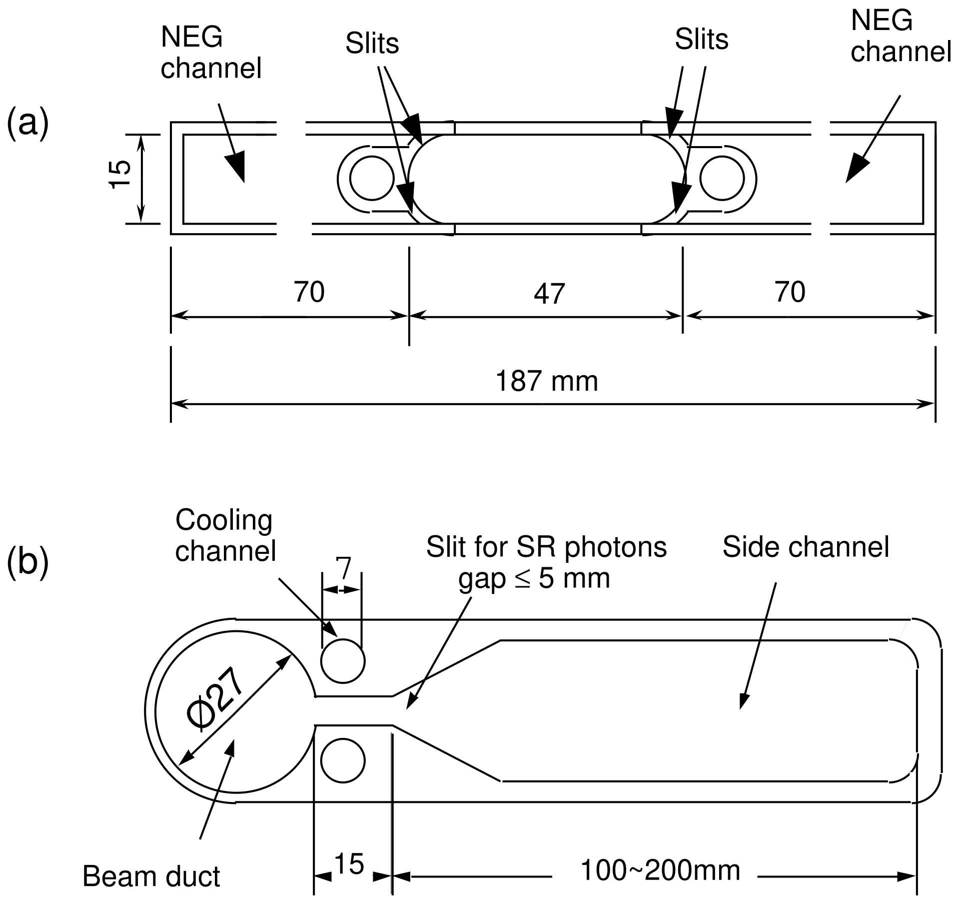

Figure 4.27: Cross sectional views of chambers (a) for the wiggler magnet (b) for the bending magnet.

In the antechamber, the maximum temperature at the surface of the copper photon absorber will reach 100 °C. The first antechamber of the bending section must absorb the power from wigglers, and thus the maximum temperature of the absorber will become several hundred degrees. Therefore, these photons are let out of the ring like SR rings do.

A prototype of 3m vacuum chamber was tested and we obtained much information to improve the production technique of the vacuum chamber. We are planning the design of almost perfect RF contact for bellows and of cooling system for the reduction of the number of absorbers.

Pumping scheme

The roughing pump system is connected to vacuum chambers by manually operated valves. The system consists of an oil-free turbomolecular pump with magnetic bearings and a rotary pump. The pump will be mounted on a cart and disconnected from the vacuum chamber during operation except for the NEG pump activation. Sputter ion pumps (SIPs) will be mainly used in the ring. They will be placed just before the photon absorber to effectively evacuate desorbed gases. The SIPs will be of 60 l/s nominal pumping speed for straight chambers and 100 l/s for antechambers. Linear NEG ribbons will be installed in two side channels of the wiggler chamber. It effectively evacuates the desorbed gases along the beam duct. Additional lumped NEG modules will be installed in the normal cell to support the SIPs.